Resolution of the ellipsoid paradox in thermodynamics

Theodore J. Yoder and Gregory S. Adkins[a)]
Franklin & Marshall College, Lancaster, Pennsylvania 17604

(Received 5 February 2011; accepted 12 May 2011)

We discuss a challenge to the second law of thermodynamics in an optical setting, in which two black bodies at strategically chosen points inside a perfectly reflecting cavity of appropriate shape apparently transfer energy asymmetrically so that one body experiences a net gain of energy at the other's expense. We show how the finite sizes of the black bodies lead to a resolution of the apparent paradox. We describe a simulation that allows us to follow the paths of individual rays and show numerically that the second law requirement of energy balance is satisfied. We also demonstrate that the energy balance condition is satisfied in the more general situation where the cavity and black bodies are of arbitrary shape.
[DOI: 10.1119/1.3596430]

I. INTRODUCTION

Imagine a perfectly reflecting cavity composed of a section of an ellipsoid E_1 [see Fig. 1(a)] with foci at A and B, a section of a sphere S centered at B, and a section of a larger ellipsoid E_2 also with foci A and B. At the focal points A and B place two identical small black bodies at equal temperatures. If we construct the cavity so that no ray from A reaches the sphere directly, then all of the thermal energy emitted from A ends at B (in the ray optics approximation) and is absorbed there, while some of the energy emitted from B is reflected back to B by the spherical section. There is thus a net flow of energy from A to B, which could be harnessed to perform useful work. If the energy is not extracted, body B will become hotter than A. The equilibrium temperatures must satisfy $R_A^2 T_A^4 = R_B^2[1 - \Omega_s/(4\pi)]T_B^4$, where R_A and R_B are the radii of sources A and B (assumed to be equal, for now), and Ω_S is the solid angle subtended by the spherical section S as viewed from B. We conclude that there is a violation of the second law of thermodynamics and a perpetual motion machine of the second kind.

Variants of the two-ellipsoid configuration we have described have been proposed and discussed over the years.[1–17] The most common variant involves a single small ellipsoid E_1 and a sphere S as in Fig. 1(b). In this case it is not as easy to find the fraction of energy from source A that eventually reaches B and the fraction that returns to A, but it is clear that there is a net flow from A to B. The early discussions of the ellipsoid paradox that we found until that of Palmer[14] all refer to the version of Fig. 1(b).

The earliest reference to the ellipsoid paradox known to us was by Fallows in 1959,[1] who posed the paradox without suggesting a solution. Osborne[2] stated that B will "emit a correspondingly greater amount of radiant energy at each wavelength" than A to maintain energy balance. (Osborne's solution seems to imply violation of the second law.) Dryburgh[3] stated that the explanation "involves only the principle of radiation traveling with equal ease in either direction along a given path." Bisacre[4] pointed out that "the geometry of the problem breaks down" if A and B are finite bodies instead of point sources. The paradox was posed in a different context by Greenleaf,[5] and generated much discussion.[6–8] Guggenheim[6] and then Landsberg[8] summarized the correspondence and focused on a resolution based on the finite size of the sources. In an appendix to Ref. 8, Davies presented an exact calculation showing that for equal source radii in the small source limit (and for a restricted class of geometries), the effective solid angle in Fig. 1(b) at source A for emission of rays absorbed by B equals the solid angle at B for emission of rays absorbed by A. Landsberg also gave a number of historical comments about related considerations by Clausius, Kelvin, Rankine, and Gibbs. Landsberg noted that a colleague referred to the configuration of Fig. 1(b) as the "Chinese furnace," but could not track down the origin of the name. The ellipsoid paradox was posed as a "brain teaser" by Helsdon,[9] but the solution given was too brief to be clear. An expanded response was provided by Higbie[10] with some related versions of the paradox with different geometries. Boley and Scully[11] presented a detailed discussion of the paradox of Fig. 1(b), taking into account not only the internal states of atoms at A and B (assumed to have two energy states each), but also the radiation in the cavity. They found that A and B approach a common temperature at large times. Welford and Winston[12] commented that the extensive statistical mechanics treatment is unnecessary and presented the finite source size resolution to the paradox instead. Landsberg[13] followed up with a brief note containing references to prior discussions. Palmer[14] posted a clear discussion of the paradox in the form of Fig. 1(a). This document is the first one we have found to use the two-ellipsoid geometry. Unfortunately, there are no references. Palmer's version of the paradox was posted and discussed in Ref. 15. Mutalik[16,17] recently posted the Chinese furnace paradox and a resolution in the New York Times.

As mentioned, there have been several proposed resolutions to the ellipsoid paradox. One concerns the finite size of the sources. Bodies A and B must have a finite size to have a finite heat capacity, without which the paradox would become meaningless. Another resolution relaxes the idealization of a perfectly reflecting and non-absorbing shell. A physical shell would absorb to some extent and, due to its nonzero temperature, would also emit thermal radiation into the cavity. After waiting long enough, there would be equilibrium between sources and the shell at a common temperature. Other suggestions involve the ray optics approximation for energy propagation without considering diffraction, the neglect of quantum effects, and the neglect of field modes inside the cavity.

We consider the paradox in the context of ray optics inside of a perfectly reflecting shell and focus on the effects of finite size sources. We will show that their finite size is crucial, and that the paradox can be resolved simply by means

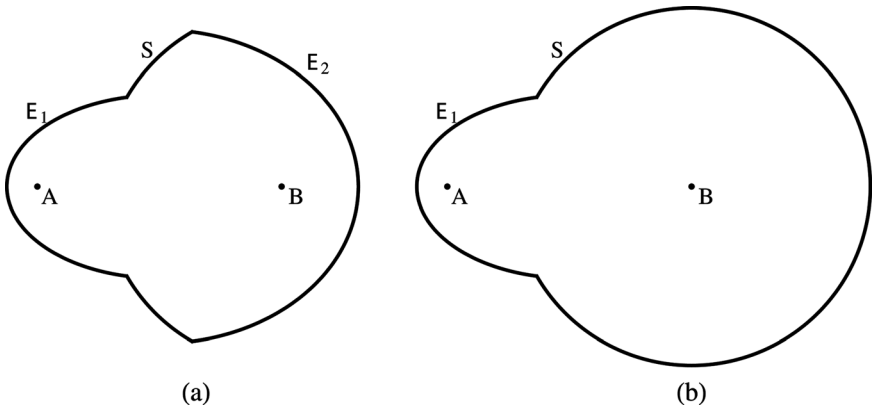

Fig. 1. Geometric configurations for two variants of the ellipsoid paradox, shown in cross-section. Sources A and B are located at the foci of an ellipsoid section E_1. Attached to E_1 is a section of a sphere S with its center at B. In the two-ellipsoid geometry of (a) there is a second and larger ellipsoid section, E_2, with the same foci as E_1. The spherical section in (a) is positioned and constrained so that no rays coming directly from A can hit anywhere on S. The "Chinese furnace" geometry of (b) is formed entirely of the ellipsoid E_1 and sphere S. The actual cavities are surfaces of revolution obtained from these cross-sections by revolution on the line containing A and B.

of geometry and ray optics, as is the consensus of many of the previous discussions of the paradox. The main point is illustrated in Fig. 2, which shows the loss of focus for rays propagating from the focal point A. These rays fail to focus precisely at point B. Depending on the size of body B, several rays miss body B and continue to make (possibly many) reflections until they reach body A or B. The paradox is resolved by the lack of focus for finite sized sources, even in the limit that the sources are small compared to the size of the cavity.

Our contribution to the resolution of the ellipsoid paradox is to verify that the second law is satisfied quantitatively so that the transfer of energy from A to B equals that from B to A for a variety of source radii and cavity configurations. Our simulation follows the propagation of rays from A to B and B to A to show that the energy transfer is the same in each direction. We can follow the path of an individual ray through sometimes hundreds of reflections to see where it is finally absorbed. We also give an analytical analysis showing exact energy flow balance in a more general geometry.

II. RAY OPTICS SIMULATION

We wrote a computer program to follow the path of an arbitrary ray emitted from either one of the sources. We used the program to verify in quantitative detail the suggestion that the resolution of the paradox resides in the finite sizes of the sources by showing that the energy emitted by source A and absorbed by B equals the energy emitted by B and absorbed by A. We found that the energy flows are equal only when the angular distribution of the emitted energy follows Lambert's emission law, which states that the angular distribution of radiated energy is proportional to $\cos\theta\, d\Omega$ where θ is the angle between the direction of emission and the surface normal and $d\Omega$ is the element of solid angle.[18] The necessity of including the $\cos\theta$ factor is not surprising given that Lambert's law is a part of the complete black body emission law, which follows from the second law of thermodynamics.

We considered the paradox in both two- and three-dimensional forms. The two-dimensional variant is simpler to set up and the behavior of rays in the two-dimensional situation is significantly easier to illustrate. The three-dimensional variant is more physical, being finite in extent, and is the version of the paradox that was originally proposed in the literature. In two dimensions, diagrams such as those of Fig. 1 are cross-sections, with infinite extent in the direction (z) transverse to the page. The sources are right circular cylinders, and the shell is formed from elliptical cylinders and another right circular cylinder. Rays are emitted in all directions from every source point, but it suffices to consider the projection of the path of the rays on the x-y plane. The z motion is a trivial trip along the z-axis. In three dimensions, the shell is the surface of revolution of the outline shown in Fig. 1 and the sources are spheres. The three-dimensional simulation is not significantly more difficult to handle than the two-dimensional case. We describe the three-dimensional simulation here.

The geometry of Fig. 1(a) can be defined by specifying just three values: the semi-major axis of the small ellipse a_1, the eccentricity of the small ellipse ϵ_1, and the angle α between the symmetry axis and a point on the spherical section S nearest to A (see the Appendix). An alternative choice

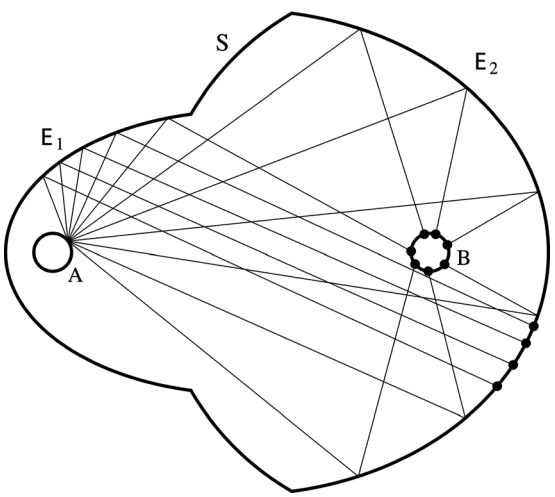

Fig. 2. A spread of 11 rays leaves body A from a point on its surface. These rays do not come to a focus at the center of body B, and several of the rays do not hit body B at all. The dots show where each ray hits after one reflection. Of the four that miss B after one reflection, three are eventually absorbed by A and one by B. Rays that reflect off E_2 must intersect body B (which in this example has the same radius as A) because the distance from the point of reflection to B is less than the distance from A to the point of reflection.

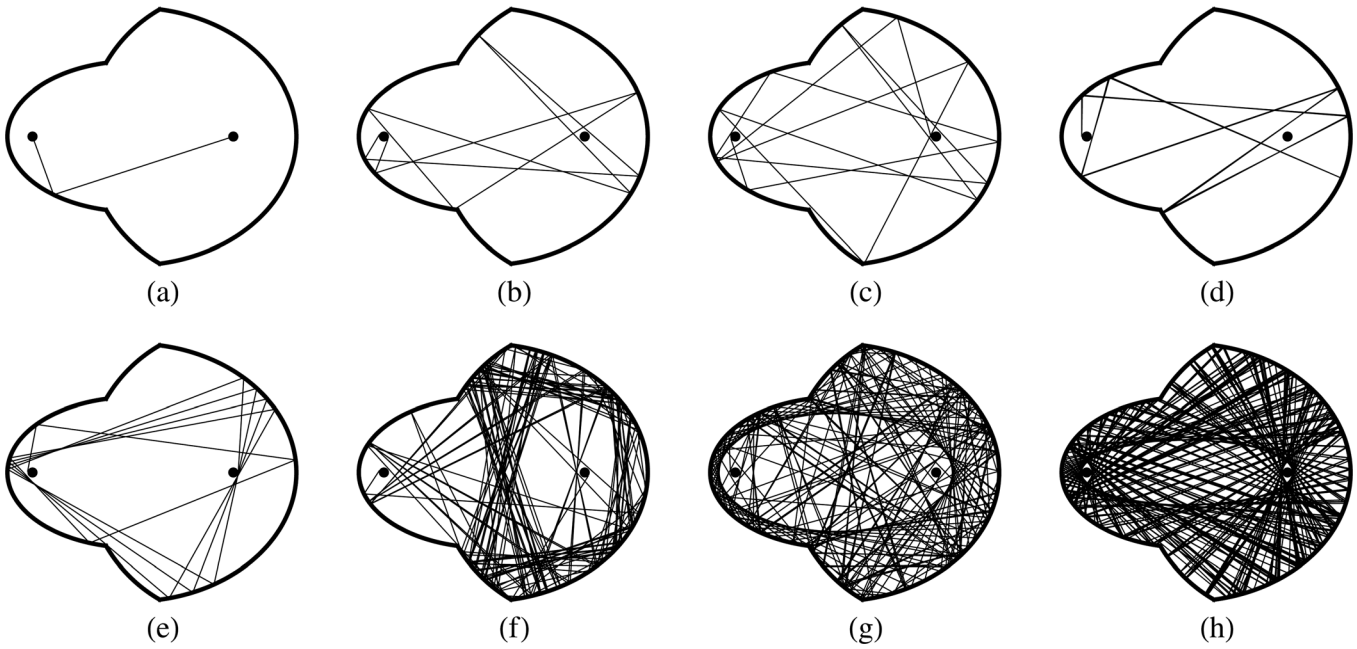

Fig. 3. Ray diagrams for typical two-dimensional paths, shown in order of increasing numbers of reflections. These paths can be thought of as two-dimensional projections of paths in the cylindrical geometry, or as special cases of the three-dimensional geometry that happen to lie in a plane. The ray shown in (a) is typical of a single-reflection path from A to B. Ray (b) bounces 8 times before returning to A. Ray (c) from B to A has 12 reflections. Ray (d) from A to A retraces its path after a reflection at nearly a right angle. Ray (e) from A to B traverses the perimeter of the cavity in a precessing triangle. Ray (f) from B to A enters a five-sided nearly resonant situation with 140 reflections. Rays (g) from B to A and (h) from A to B form some of the striking patterns that often emerge with high numbers of reflections (here 194 and 352). It is possible to find paths that nearly fill the cavity and have many thousands of reflections.

of the third parameter is $\xi = R/a_1$, where R is the radius of the spherical section of the shell. For the physical situation with non-zero source radii, the five parameters a_1, ϵ_1, α (or ξ), and the radii of the sources suffice to determine all other geometric quantities in the system.

At the heart of our simulation is an iterative step that takes a ray from an initial location $\vec{r}_i = (x_i, y_i, z_i)$ inside (or on the inside surface of) the cavity to a final location $\vec{r}_f = (x_f, y_f, z_f)$ on one of the surfaces. The initial direction of the ray is specified by a direction unit vector $\hat{u}_i = (u_{xi}, u_{yi}, u_{zi})$. After one step the ray will either be absorbed by A or B if it intercepts one of them, or it will be reflected by the inner surface of E_1, E_2, or S. It will have a new position, and if reflected, a new direction unit vector determined using the law of reflection. For each initial set $\vec{r}_i$, $\hat{u}_i$ the path of the ray is given parametrically by

$$\vec{r}(\lambda) = \vec{r}_i + \lambda \hat{u}_i. \tag{1}$$

In three dimensions, let the foci A and B define the x-axis. The equation for an ellipsoid centered at $\vec{r}_0 = (x_0, y_0, z_0)$ with circular x cross-section is

$$\frac{(x-x_0)^2}{a^2} + \frac{(y-y_0)^2}{b^2} + \frac{(z-z_0)^2}{b^2} = 1. \tag{2}$$

For the surfaces E_1, E_2, and S, the values of a and b depend only on the three parameters a_1, ϵ_1, and α (see the Appendix). We have $a = b = R_A$ for source A and $a = b = R_B$ for B. The solution for the intersections of the ray with any one of these particular surfaces proceeds as follows. Replacing x, y, and z in Eq. (2) by $x(\lambda)$, $y(\lambda)$, and $z(\lambda)$ given by Eq. (1) results in an equation quadratic in λ. Solving this equation yields values for λ at which the ray (1) intersects the ellipsoid (2). We next need to remove solutions that represent the intersection of the ray with any parts of the ellipsoid that are not involved in the construction of the cavity. Also, we are interested only in positive solutions, because, by definition, rays move forward along $\hat{u}_i$, so any negative values for λ are deleted.

We used this method to assemble a list of positive values for λ for the first intersection of the ray with each of the surfaces: A, B, E_1, E_2, and S. If a particular ray does not intersect one of the surfaces, we added $\lambda_{\max}$ to the list of candidates instead, where $\lambda_{\max}$ is greater than the largest dimension of the cavity. Thus, we have a set of positive λ values, one for each surface involved in constructing the cavity and two for the sources, from which we choose the minimum $\lambda_{\min}$ and advance the ray to the new position $\vec{r}_f = \vec{r}_i + \lambda_{\min}\hat{u}_i$. If $\vec{r}_f$ is on A or B the process stops. Otherwise, the new direction unit vector is

$$\hat{u}_f = \hat{u}_i - 2\hat{n}(\hat{n} \cdot \hat{u}_i), \tag{3}$$

where $\hat{n}$ is the outward-pointing unit normal to the reflecting surface at $\vec{r}_f$. A convenient way to find the normal is to use the fact that it is proportional to $\vec{\nabla}\Phi$, where $\Phi = 0$ is the equation of the surface of interest. We iterate the basic step until the ray intersects A or B, at which point it is absorbed.

Some trajectories are shown in Fig. 3. Although we have shown some interesting paths, most paths have just one reflection like that of Fig. 3(a). The next most common has two reflections. For purposes of calculating means and standard deviations of quantities of interest, we computed 12 samples of 200,000 two-dimensional paths starting at A and ending at B, and the same number from B to A, for each geometry. The initial angles θ (the position of the emitted ray

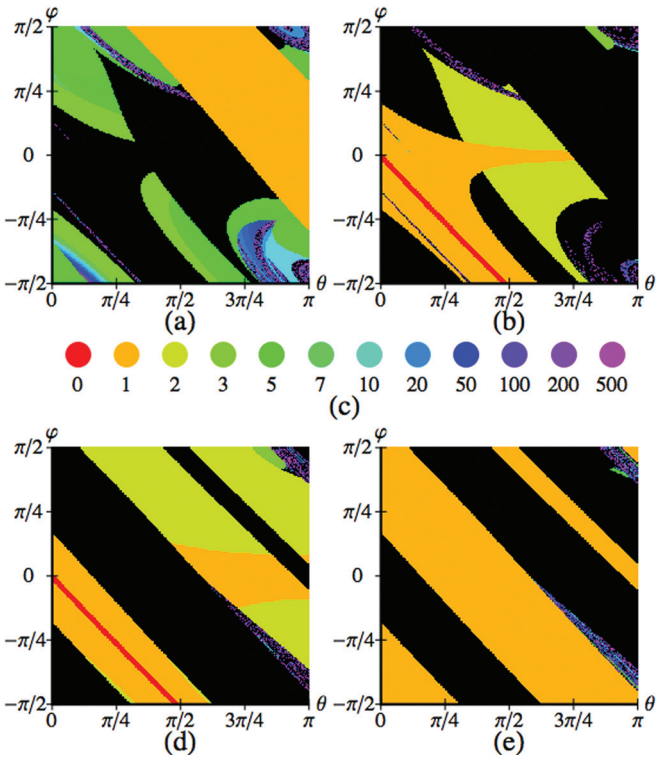

Fig. 4. (Color) Examples of the fate and number of reflections for rays traveling between the sources in the two-dimensional ellipsoid geometry with $a_1=2.5$, $\epsilon_1=0.9$, $\xi=0.9$, and $R_A=R_B=0.2$. Parts (a) and (b) show the destinations of rays given off by source A. The colors in (a) show the number of reflections undergone by rays from A that end on A (with black for rays ending on B) and (b) carries the same information for rays from A to B (with black for rays ending on A). The angles identify which ray is being followed: θ describes the position on the source of the emitted ray and ϕ gives its angle with respect to the normal. The angles are defined so that $\theta=0$ is the position on one source closest to the other source, and both θ and ϕ increase in the counterclockwise direction. Rays with $-\pi\le\theta\le 0$ duplicate those with $0\le\theta\le\pi$, and so are not shown. Most rays from A to B undergo one or two reflections—a few suffer many reflections. A sampling of the colors used to represent numbers of reflections is shown on a continuous logarithmic scale in (c). Parts (d) and (e) give the same information as (a) and (b), only for rays from B to A in (d) and B to B in (e).

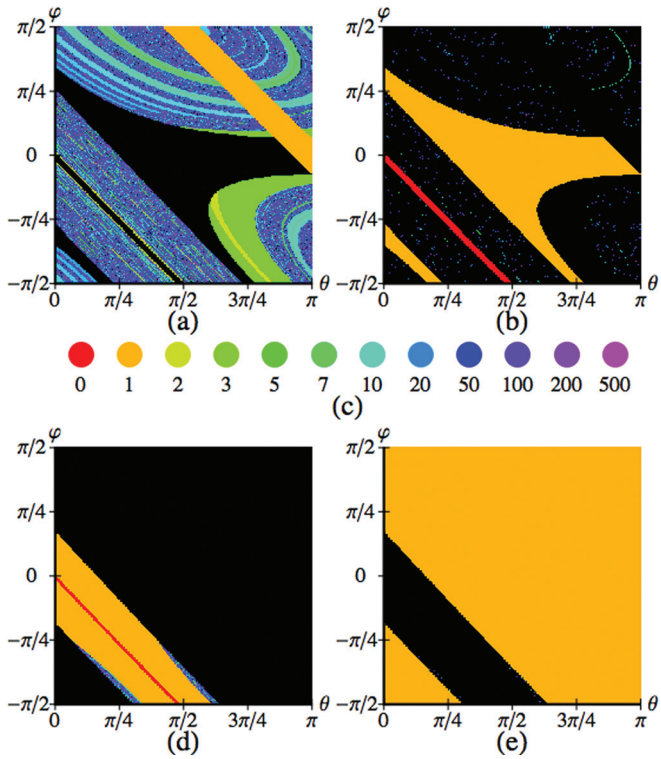

Fig. 5. (Color) The same information as in Fig. 4, except for the Chinese furnace geometry with $a_1=2.5$, $\epsilon_1=0.8$, $\alpha=\pi/4$, $R_A=0.1$, and $R_B=0.2$. Most of the rays from A to B and from B to A suffer only zero or one reflections while a few undergo many reflections. Many of the rays from A to A have complicated paths.

on the source) and ϕ (the angle of the emitted ray with respect to the normal) were chosen randomly subject to the Lambert emission law. Only a small percentage of paths have more than 10 or 12 reflections. Occasionally an extremely long path occurs, and, as a result, the mean number of reflections is unexpectedly large. A detailed balance principle holds, and the numbers for paths from A to B are the same (within uncertainties) as for paths from B to A. For example, for the two-ellipsoid geometry of Fig. 1(a) with $a_1=2.5$, $\epsilon_1=0.8$, $\alpha=\pi/4$, and with source radii $R_A=R_B=0.1$, the fractions of paths from A to B having 0, 1,…, 12 reflections are 0.0134(1), 0.6700(4), 0.2896(3), 0, 0, 0.0032(1), 0.0054(1), 0, 0.0007(1), 0.0079(1), 0, 0.0022(1), and 0.0034(1), respectively. (The 1σ uncertainties in the last digit are shown in parentheses.) The average number of reflections is 9.86(17). The numbers for B to A are the same within the uncertainty.

From the examples shown in Fig. 3 we see that a ray path can be extremely sensitive to numerical inaccuracy, introduced, for example, by round-off errors. For instance, a slight variation in the path could change the 352 reflection path of Fig. 3(h) to a much shorter one, and lead to absorption by one source instead of the other. This sensitivity can affect even short paths, but it is much more likely for long ones. Fortunately, long paths are rare. We found noticeable divergences between the paths generated by different implementations of the ray tracing simulation after a few hundred reflections, which leads us to distrust the details of the very long paths. Because most paths are short, our results for numerical integrals are trustworthy within the given uncertainty.

The paths of rays leaving the sources obtained using our two-dimensional simulations are illustrated in Figs. 4 and 5. These figures show the final destinations of rays emitted from source A in parts (a) and (b) and from B in parts (d) and (e) as functions of the angles θ and ϕ of the emitted ray. Part (a) encodes the number of reflections undergone by any particular ray emitted from A and returning to A, as does part (b) for rays from A to B. Parts (d) and (e) give analogous information for rays emitted from B. The rays of particular interest are the ones from A to B (shown in colors in part (b) and from B to A [in color in part (d)]. The red lines in (b) and (d) represent rays aimed straight at the other source that reach it without reflection.

III. ENERGY FLOW RESULTS

We used our ray optics simulation to determine the energy flow rate between the sources for various geometries. The power emitted from the area element dA in the frequency range $d\nu$ and into the solid angle $d\Omega=\sin\theta d\theta d\phi$ by a black body source at temperature T is

$$dP = I(\nu, T) d\nu dA \cos\theta d\Omega, \tag{4}$$

where

$$I(\nu, T) = \frac{2h\nu^3}{c^2} \frac{1}{e^{h\nu/kT} - 1} \tag{5}$$

is the Planck distribution. Here θ is the angle between the normal to the surface and the direction of the radiation. The factor $\cos\theta$ is present because black bodies satisfy the Lambert emission law.[18] (A consequence of the presence of $\cos\theta$ is the fact that the radiance of black bodies is independent of viewing angle.) The power transfer from A to B in frequency range $d\nu$ can be expressed as

$$dP_{A\to B} = d\tilde{P}_A p(A \to B), \tag{6}$$

where the total power radiated from A in frequency range $d\nu$ is $d\tilde{P}_A = I(\nu, T) d\nu (S_A)(\pi)$, with S_A the area of source A, $\pi = \int d\Omega \cos\theta = \int_0^{2\pi} d\phi \int_0^{\pi/2} d\theta \sin\theta \cos\theta$, and $p(A \to B)$ is the probability that a ray emitted with the $\cos\theta\, d\Omega$ distribution is eventually absorbed by B. The quantities that we actually calculated were the probabilities $p(A \to B)$ and $p(B \to A)$. We found these to be equal (to within numerical uncertainties) for sources of equal radii. If the energy transfer balances for each frequency ($dP_{A\to B} = dP_{B\to A}$), we would expect to find

$$S_A p(A \to B) = S_B p(B \to A) \tag{7}$$

or

$$r \equiv \left(\frac{R_A}{R_B}\right)^{d-1} \frac{p(A \to B)}{p(B \to A)} = 1, \tag{8}$$

for the two-dimensional ($d = 2$) and three-dimensional ($d = 3$) cases. We ran 2^5 simulations using the two-ellipsoid or Chinese furnace configurations, and the two- or three-dimensional geometries. The parameter sets are $a_1 = 2.5$, $\epsilon_1 = 0.8$, and $\alpha = \pi/4$, or $a_1 = 2.5$, $\epsilon_1 = 0.9$, and $\xi = 0.9$; 0.1 or 0.2 for R_A; and 0.1 or 0.2 for R_B. Our numerical results for r are consistent with unity to within our uncertainties of a few parts per thousand. (For each case we did 12 runs of 400,000 rays emerging from each of the two sources.) We conclude that the rates of energy flow from A to B and from B to A are equal, and that there is no paradox.

IV. ANALYTIC ANALYSIS

In this section we give an analytic demonstration for the energy balance between black bodies in reflecting cavities. The analytic argument is not based on specific geometric features such as spherical sources or specially designed cavities, and is a significant generalization of the previous results. Consider a perfectly reflecting cavity of any shape containing two black bodies A and B. Rays connecting A and B undergo some number $n = 0,1,2,\ldots$ of reflections, and rays with a given value of n can be grouped so that all of the rays within a given group can be continuously deformed into one another. For example, there are two groups of one-reflection rays between A and B in Fig. 1(a): those hitting E_1 and those hitting E_2. The n-reflection paths from A to B can be partitioned into infinitesimal elements all of which have propagation angles that are within $O(\epsilon)$ (where ϵ is an infinitesimal angle) of each other. A convenient way to perform this partition is to represent all of the n-reflection rays leaving one of the black bodies on a four-dimensional phase diagram (two space and two direction coordinates) and partition the n-reflection region into differential elements of $O(\epsilon L)$ in each spatial direction, where L is a length characteristic of the sources. For example, a one-reflection bundle of rays from S_1 on A to S_3 on B is shown in Fig. 6.

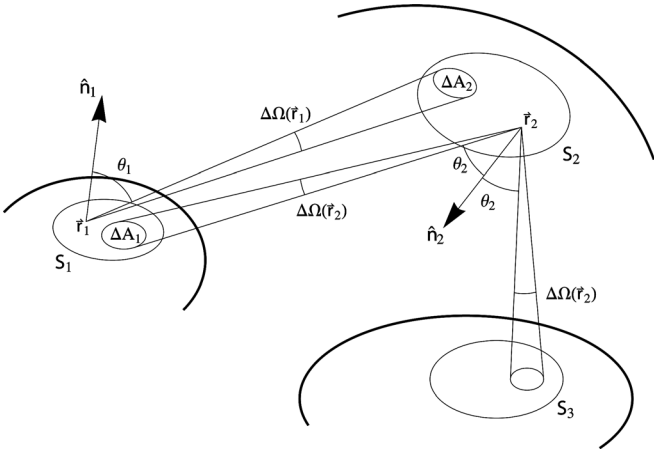

Fig. 6. A bundle of one-reflection rays from S_1 on A to S_3 on B by way of S_2 on the reflecting envelope. The sizes of S_1, S_2, S_3 and, consequently, the sizes of the solid angles are exaggerated for clarity. The regions S_1, S_2, and S_3 are infinitesimal, so all rays from S_1 to S_2 are approximately parallel, as are all rays from S_2 to S_3. The normals $\hat{n}_1$ and $\hat{n}_2$ to S_1 and S_2 are shown along with some representative rays.

We now prove the central result that the power P_1 leaving S_1 and arriving at S_3 is the same as the power P_3 leaving S_3 and arriving at S_1 as long as the temperatures of bodies A and B are the same. The power emitted by S_1 in frequency range dv equals the radiance factor R_1 times the étendue,[19]

$$P_1 = R_1 \int_{S_1} d^2 r_1 \int d\Omega_1 \cos\theta_1, \tag{9}$$

where S_1 is an infinitesimal element of area on body A and $R_1 \equiv I(\nu, T_1) d\nu$ as in Eq. (4). The points of S_1 are labeled by the vector $\vec{r}_1$, and $d^2 r_1$ is the element of area on S_1. At each point $\vec{r}_1$ on S_1 rays are emitted within a small range of directions described by $d\Omega_1$. The exact directions and total solid angle of rays emitted from point $\vec{r}_1$ are not the same for all points in S_1 even though S_1 is an infinitesimal element, and hence the need for the integrals in Eq. (9). The area element S_1 is small enough that the normal vector $\hat{n}_1$ and the $cos\theta_1$ factor for all rays in the bundle can be taken to be constant over S_1. The integral over the solid angle can be done, giving the total solid angle $\Delta\Omega(\vec{r}_1)$ for all rays in the bundle that are emitted from the point $\vec{r}_1$. (Note that $\Delta\Omega(\vec{r}_1)$ is of $O(\epsilon^2)$, and the étendue is of $O(\epsilon^4)$).

Our first task is to show that the étendue of the emitted rays from S_1 is the same as that of the received rays at S_2. That is, we need to show that

$$\int_{S_1} d^2 r_1 \Delta\Omega(\vec{r}_1) \cos\theta_1 = \int_{S_2} d^2 r_2 \Delta\Omega(\vec{r}_2) \cos\theta_2. \tag{10}$$

Consider all of the rays leaving point $\vec{r}_1$ on S_1 in the infinitesimal bundle of rays under consideration. These rays fill an

area element ΔA_2 on S_2. The solid angle $\Delta\Omega(\vec{r}_1)$ can be expressed as the transverse projection of ΔA_2 divided by r_{12}^2, where r_{12} is the distance between S_1 and S_2,

$$\Delta\Omega(\vec{r}_1) = \frac{\cos\theta_2 \Delta A_2}{r_{12}^2} = \frac{\cos\theta_2}{r_{12}^2}\int_{S_2} d^2 r_2 \Theta(\vec{r}_1, \vec{r}_2). \tag{11}$$

We have introduced the Θ function that vanishes unless the points $\vec{r}_1$ and $\vec{r}_2$ are connected by a ray in the bundle,

$$\Theta(\vec{r}_1, \vec{r}_2) = \begin{cases} 1 & \text{if a ray from } \vec{r}_1 \text{ reaches } \vec{r}_2 \\ 0 & \text{otherwise} \end{cases}. \tag{12}$$

Similarly, the solid angle subtended by rays reaching a generic point $\vec{r}_2$ in S_2 can be written as

$$\Delta\Omega(\vec{r}_2) = \frac{\cos\theta_1 \Delta A_1}{r_{12}^2} = \frac{\cos\theta_1}{r_{12}^2}\int_{S_1} d^2 r_1 \Theta(\vec{r}_1, \vec{r}_2). \tag{13}$$

Thus the étendue for rays arriving at S_2 is

$$\int_{S_2} d^2 r_2 \Delta\Omega(\vec{r}_2)\cos\theta_2 = \frac{\cos\theta_1 \cos\theta_2}{r_{12}^2}\int_{S_2} d^2 r_2 \times \int_{S_1} d^2 r_1 \Theta(\vec{r}_1, \vec{r}_2), \tag{14}$$

which, after reversing the order of integration, is the same as the étendue for rays leaving S_1. The étendue for the reflected radiation leaving S_2 is the same as for the radiation arriving there, because the angles (for example, θ_2 in Fig. 6) and solid angles (for example, $\Delta\Omega(\vec{r}_2)$ in Fig. 6) are both preserved under reflection. An analogous argument shows that the étendue of the rays arriving at S_3 equals that of rays leaving S_2, and thus is the same as the étendue of the rays leaving S_1. Due to étendue conservation and the assumption that no power is lost upon reflection, we can express the power incident on S_3 as

$$P_{3,\text{in}} = R_1 \int_{S_3} d^2 r_3 \Delta\Omega(\vec{r}_3)\cos\theta_3. \tag{15}$$

All is absorbed because B is an ideal absorber.

We now consider the time-reversed bundle of rays from S_3 back to S_1. Every ray in the original bundle corresponds to a ray in the reversed bundle having the same path but traced out in the opposite direction. The power radiated from S_3 along the reversed path is

$$P_{3,\text{rad}} = R_3 \int_{S_3} d^2 r_3 \Delta\Omega(\vec{r}_3)\cos\theta_3, \tag{16}$$

where $R_3 = I(\nu, T_3)d\nu$ is the radiance factor of body B. The incident and radiated powers are balanced in every frequency range if and only if $R_1 = R_3$, which holds exactly when the temperatures of A and B are identical.

The argument given for one-reflection paths generalizes to paths with any number of reflections. Thus, after integration of all the infinitesimal ray bundles, we obtain the final result that the energy flow from A to B equals that from B to A as long as the temperatures of A and B are equal, no matter what the shapes of the sources or the cavity. Lambert's emission law is an essential element of this delicate balance. Without the $\cos\theta_1$ factor in the emitted power in Eq. (9) the proof would fall apart. Specifically, because $\cos\theta$ appears naturally in the solid angle calculations (11) and (13), it has to be in Eqs. (9) and (10) as well. The detailed balance that we noticed in the simulations—that the energy flow balances for each number of reflections separately—is a consequence of the general demonstration. In addition, the general demonstration implies energy flow balance on the finer level of infinitesimal bundles of rays.

ACKNOWLEDGMENTS

The authors would like to thank Nina Byers, Amy Lytle, Etienne Gagnon, and Calvin Stubbins for useful discussions and suggestions, and the reviewers for helpful comments. We acknowledge the support of Franklin & Marshall College through the Hackman Scholars program.

APPENDIX: GEOMETRY OF THE PARADOX

We demonstrate an explicit construction of the geometry of the paradox. The construction of the geometry of Fig. 1(b) should be evident from the construction of the more complicated Fig. 1(a), which we now discuss in detail. Three parameters are necessary to specify the geometry of the shell. One, which can be taken to be the semi-major axis a_1 of the

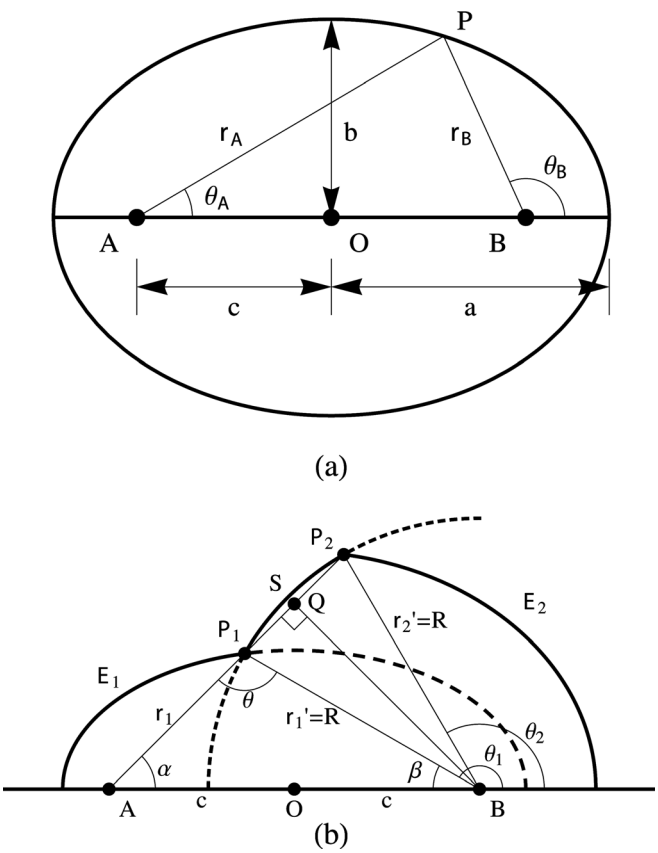

Fig. 7. (a) An ellipse with semi-major axis a and semi-minor axis b. The foci and center are at A, B, and O, and c is half the distance between the foci. A generic point P is on the ellipse. The ellipse has eccentricity $\epsilon = 0.7$. (b) The construction of the ellipsoid paradox geometry using a_1, ϵ_1, and α as parameters. The continuations of ellipsoid cross-section E_1 and sphere cross-section S are shown as dashed lines.

small ellipse E_1, serves to set the overall scale and can have any positive value. For the second parameter we choose the eccentricity ϵ_1 of the small ellipse. There are two choices of the third parameter: the angle α shown in Fig. 7(b) or the ratio $\xi = R/a_1$, where R is the radius of the spherical section. We show the construction in terms of α first.

As a quick review, an ellipse of semi-major axis a, semi-minor axis b, and eccentricity ϵ is shown in Fig. 7(a). The sum of the distances from the foci to any point P on the perimeter is given by

$$r_A + r_B = 2a. \tag{A1}$$

Half the distance between the foci is given by $c = \epsilon a$, and because $a^2 = b^2 + c^2$, it follows that $b = a\sqrt{1-\epsilon^2}$. The polar ellipse equation takes either of the forms

$$r_A = \frac{b^2}{a - c\cos\theta_A}, \tag{A2a}$$

$$r_B = \frac{b^2}{a + c\cos\theta_B}. \tag{A2b}$$

For our construction [see Fig. 7(b)] we choose $a_1 > 0$ and parameters ϵ_1 and α such that $0 < \epsilon_1 < 1$ and $0 < \alpha < \pi/2$, subject to a constraint to be specified. Let A and B be the two foci and O the center of the small ellipse E_1. Points P_1 and P_2 delimiting the spherical segment S are on a line from A at angle α to the centerline given parametrically by

$$\vec{r}(\lambda) = (x(\lambda), y(\lambda)) = (-c, 0) + \lambda(\cos\alpha, \sin\alpha), \tag{A3}$$

with the origin at O and $c = \epsilon_1 a_1$ half the distance between the foci. Points P_1 and P_2 also lie on the circle

$$(x - c)^2 + y^2 = R^2 \tag{A4}$$

of radius R with center at B. The simultaneous solutions to Eqs. (A3) and (A4) are

$$\lambda = 2c\cos\alpha \pm \sqrt{R^2 - 4c^2\sin^2\alpha}. \tag{A5}$$

The distance Δ between P_2 and P_1 is

$$\Delta = r_2 - r_1 = 2\sqrt{R^2 - 4c^2\sin^2\alpha}, \tag{A6}$$

where r_1 and r_2 are the lengths of the line segments $\overline{AP_1}$ and $\overline{AP_2}$, respectively. We can find the radius R of the sphere by use of the equation,

$$2a_1 = r_1 + r_1' = r_1 + R, \tag{A7}$$

where $r_1' = R$ is the length of $\overline{BP_1}$, and the parametric equation (A2a)

$$r_1 = \frac{b_1^2}{a_1 - c\cos\alpha} = \frac{(1-\epsilon_1^2)a_1}{1 - \epsilon_1\cos\alpha}, \tag{A8}$$

so that

$$R = 2a_1 - r_1 = \left(\frac{1 - 2\epsilon_1\cos\alpha + \epsilon_1^2}{1 - \epsilon_1\cos\alpha}\right)a_1. \tag{A9}$$

The semi-major axis of the large ellipse E_2 can be found from the equation,

$$\begin{aligned} 2a_2 &= r_2 + r_2' = r_1 + 2\sqrt{R^2 - 4c^2\sin^2\alpha} + R \\ &= 2a_1 + 2\sqrt{R^2 - 4c^2\sin^2\alpha}, \end{aligned} \tag{A10}$$

where $r_2' = R$ is the length of $\overline{BP_2}$, so that

$$a_2 = a_1 + \sqrt{R^2 - 4c^2\sin^2\alpha}. \tag{A11}$$

The large ellipse has the same foci as the small one, and thus the value of c is the same for both. The eccentricity of E_2 is

$$\epsilon_2 = \frac{c}{a_2} = \epsilon_1\frac{a_1}{a_2}. \tag{A12}$$

We also need the angles θ_1 and θ_2, which are found by inverting the parametric equations in Eq. (A2),

$$\theta_1 = \cos^{-1}\left[\frac{1}{\epsilon_1}\left((1-\epsilon_1^2)\frac{a_1}{R} - 1\right)\right], \tag{A13a}$$

$$\theta_2 = \cos^{-1}\left[\frac{1}{\epsilon_2}\left((1-\epsilon_2^2)\frac{a_2}{R} - 1\right)\right]. \tag{A13b}$$

The condition on the choice of ϵ_1 and α comes from the requirement that the point Q, where the perpendicular from B meets the half-line $\overrightarrow{AP_1}$, lies outside of the small ellipse. Point Q lies outside of E_1 because Q is the midpoint of the chord $\overline{P_1P_2}$, which lies outside of E_1. Because the angle AQB is a right angle, the angle θ is greater than $\pi/2$. We see that the possible positions of P_1 on E_1 are constrained so that $\theta > \pi/2$. It is a general property of ellipses that

$$\epsilon_1 = \frac{\sin\theta}{\sin\alpha + \sin\beta}, \tag{A14}$$

which can be shown using the law of sines on triangle ABP_1 along with the ellipse condition $r_1 + r_1' = 2a_1$. Corresponding to the extreme value $\theta = \pi/2$ there are extreme values of α, either a maximum (with P_1 closer to A) or a minimum (with P_1 closer to B), which we denote by $\bar{\alpha}$. In either case we have $\beta = \pi/2 - \bar{\alpha}$ and Eq. (A14) becomes

$$\epsilon_1 = \frac{1}{\cos\bar{\alpha} + \sin\bar{\alpha}} = \frac{1}{\sqrt{1 + \sin(2\bar{\alpha})}}. \tag{A15}$$

For a given value of ϵ_1 an acceptable value of α must lie between the two solutions $\bar{\alpha}$ to Eq. (A15) in the range $(0, \pi/2)$. (These solutions must exist for the construction to work, and hence we need $\epsilon_1 > 1/\sqrt{2}$.) Another expression of this condition is that, for a given value of α in the range $(0, \pi/2)$, the eccentricity must satisfy

$$\epsilon_1 > \frac{1}{\sqrt{1 + \sin(2\alpha)}}. \tag{A16}$$

An alternate choice of parameters[14] takes a_1, ϵ_1, and $\xi = R/a_1$ as fundamental. We can invert Eq. (A9) to find α in terms of these parameters ϵ_1 and ξ,

$$\alpha = \arccos\left(\frac{1 - \xi + \epsilon_1^2}{\epsilon_1(2 - \xi)}\right), \tag{A17}$$

and then the construction of the spherical section and the large ellipse proceeds as before. The allowable range of ξ is given by $2\epsilon_1 \sin\bar{\alpha}_1 < \xi < 2\epsilon_1 \cos\bar{\alpha}_1$, where $\bar{\alpha}_1$ is the smallest positive solution of Eq. (A15).

[a]Electronic mail: gadkins@fandm.edu

[1]J. C. Fallows, "Heat transfer paradox," The New Scientist **5**, 1156 (1959).
[2]R. V. Osborne, "Heat transfer paradox," The New Scientist **5**, 1310 (1959).
[3]P. M. Dryburgh, "Heat transfer paradox," The New Scientist **6**, 113 (1959).
[4]G. H. Bisacre, "Heat transfer paradox," The New Scientist **6**, 113 (1959).
[5]J. Greenleaf, "A fallacy in the second law of thermodynamics?," Bull. Inst. Phys. Phys. Soc. London **17**, 253 (1966).
[6]E. A. Guggenheim, "A fallacy in the second law of thermodynamics?," Bull. Inst. Phys. Phys. Soc. London **17**, 332 (1966).
[7]The Editor, "A fallacy in the second law of thermodynamics?," Bull. Inst. Phys. Phys. Soc. London **18**, 22 (1967).
[8]P. T. Landsberg, "A fallacy in the second law of thermodynamics?," Bull. Inst. Phys. Phys. Soc. London **18**, 228–231 (1967).
[9]R. M. Helsdon, "Brain teaser," Phys. Educ. **7**, 414, 446 (1972).
[10]J. Higbie, "Chinese furnace," Phys. Educ. **9**, 14–15 (1974).
[11]C. D. Boley and M. O. Scully, "The statistical mechanical resolution of a thermodynamic 'paradox'," J. Stat. Phys. 24, 159–174 (1981).
[12]W. T. Welford and R. Winston, "The ellipsoid paradox in thermodynamics," J. Stat. Phys. **28**, 603–606 (1982).
[13]P. T. Landsberg, "The ellipsoid paradox of thermodynamics," J. Stat. Phys. **34**, 357 (1984).
[14]L. H. Palmer, "An optical perpetual motion machine of the second kind," <www.lhup.edu/~dsimanek/museum/sucker.pdf>. Also see the discussion by D. Simanek at <http:lhup.edu/~dsimanek/museum/advanced.htm>.
[15]W. Wu, "Ellipsoid power generation," <www.ocf.berkeley.edu/~wwu/riddles/hard.shtml#ellipsoidPowerGeneration>.
[16]P. Mutalik, "Monday puzzle: Getting something for nothing," New York Times, <tierneylab.blogs.nytimes.com/2010/2002/22/monday-puzzle-getting-something-from-nothing/>.
[17]P. Mutalik, "The second law strikes back," New York Times, <tierneylab.blogs.nytimes.com/2010/03/05/the-second-law-strikes-back/>.
[18]G. Brooker, *Modern Classical Optics* (Oxford University Press, Oxford, 2003), p. 249.
[19]The étendue of an infinitesimal pencil of rays emerging from a source area dS at angle θ with respect to the normal and with all rays confined to a common solid angle $d\Omega$ is $n^2 dS \cos\theta\, d\Omega$, where n is the index of refraction of the medium. For our use, $n = 1$.

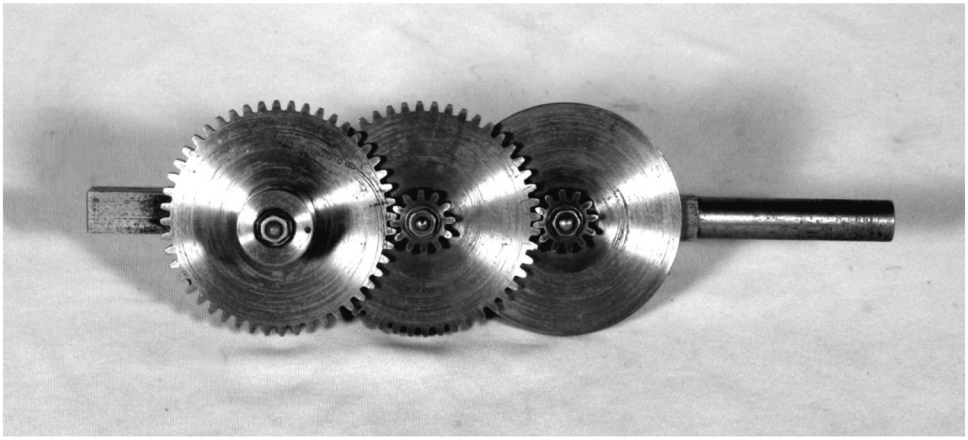

Geared Wheels. From the 1929 catalogue of the Central Scientific Company of Chicago: ″Geared Wheels. A train of gears consisting of two wheels about 7 cm in diameter with pinions of ¼ the diameter of the wheels, and a third wheel of the same size with drum of the same diameter, giving a mechanical advantage of 64. Mounted on a 13 mm square rod turned round at the end for 6 cm, for use with right angle clamp. All metal, white nickel-plated and lacquered ... $9.00″ The left-hand wheel has a pulley groove turned in its edge, and the hole allows a cord to be attached. The drum on the right-hand wheel also has a small hole for attaching a cord. The bearings are simple sleeves. In use, weights are attached to the lower ends of the cords to show that the actual mechanical advantage is 64. This apparatus is in the Greenslade Collection. (Notes and photograph by Thomas B. Greenslade, Jr., Kenyon College)